

CHEMISTRY

A European Journal

A Journal of



Accepted Article

Title: Structural and Mechanistic Insights into Development of Chemical Tools to Control Individual and Inter-related Pathological Features in Alzheimer's Disease

Authors: Hyuck Jin Lee, Kyle Korshavn, Younwoo Nam, Juhye Kang, Thomas Paul, Richard Kerr, Il Seung Yoon, Mehmet Ozbil, Kwang S. Kim, Brandon Ruotolo, Rajeev Prabhakar, Ayyalusamy Ramamoorthy, and Mi Hee Lim

This manuscript has been accepted after peer review and appears as an Accepted Article online prior to editing, proofing, and formal publication of the final Version of Record (VoR). This work is currently citable by using the Digital Object Identifier (DOI) given below. The VoR will be published online in Early View as soon as possible and may be different to this Accepted Article as a result of editing. Readers should obtain the VoR from the journal website shown below when it is published to ensure accuracy of information. The authors are responsible for the content of this Accepted Article.

To be cited as: *Chem. Eur. J.* 10.1002/chem.201605401

Link to VoR: <http://dx.doi.org/10.1002/chem.201605401>

Supported by
ACES

WILEY-VCH

Structural and Mechanistic Insights into Development of Chemical Tools to Control Individual and Inter-related Pathological Features in Alzheimer's Disease

Hyuck Jin Lee,^[a] Kyle J. Korshavn,^[b] Younwoo Nam,^[c] Juhye Kang,^[c] Thomas J. Paul,^[d] Richard A. Kerr,^[b] Il Seung Youn,^[c] Mehmet Ozbil,^[d] Kwang S. Kim,^[c] Brandon T. Ruotolo,^[b] Rajeev Prabhakar,^{*[d]} Ayyalusamy Ramamoorthy^{*[b,e]} and Mi Hee Lim^{*[c]}

Abstract: To elucidate the involvement of individual and inter-related pathological factors [*i.e.*, amyloid- β (A β), metals, and oxidative stress] in the pathogenesis of Alzheimer's disease (AD), chemical tools have been developed. Characteristics required for such tool construction, however, have not been clearly identified; thus, the optimization of available tools or new design has been limited. Herein, we report key structural properties and mechanisms that can determine tools' regulatory reactivities with multiple pathogenic features found in AD. We built up a series of small molecules *via* rational structural selection and variations [(i) location and number of an A β interacting moiety; (ii) metal binding site; (iii) denticity and structural flexibility] onto the framework of a tool useful for *in vitro* and *in vivo* metal-A β investigation. Detailed biochemical, biophysical, and computational studies using our chemical series were able to provide a foundation of how to originate molecular formulas to devise chemical tools capable of controlling the reactivities of various pathological components through distinct mechanisms. Overall, our multidisciplinary investigations illustrate a structure-mechanism-based strategy of tool invention for such a complicated brain disease, AD.

Introduction

Alzheimer's disease (AD) is a progressive and fatal brain

disorder that is defined by progressive neuronal loss and cognitive defects.^[1] Due to the unclear and complicate etiology of AD, a cure for the disease has not been discovered. Amyloid- β (A β) peptides are suggested to be associated with AD pathogenesis since misfolded A β aggregates are primary components of senile plaques found in the AD-afflicted brain (amyloid cascade hypothesis).^[1,2] Upon the proteolytic cleavage of amyloid precursor protein (APP) by β - and γ -secretases, A β peptides are produced [two major isoforms, A β_{40} and A β_{42} (*ca.* 90% and 9% in the brain, respectively), which are aggregation-prone to form aggregates from various-sized oligomers to mature fibrils].^[1a-c,2] Based on recent findings, soluble A β oligomers are observed to be toxic; however, a relationship between A β conformations and toxicity remains uncertain.^[1c,2] Moreover, the AD-affected brain exhibits highly concentrated metal ions within senile plaques [*e.g.*, *ca.* 0.4 mM for Cu^{II}, 1.0 mM for Zn^{II}, 0.9 mM for Fe^{III}].^[1d,3] Previous *in vitro* studies present that these metal ions [particularly, Cu^{II} and Zn^{II}] can interact with A β peptides and facilitate peptide aggregation. Furthermore, complexes of A β and redox-active metal ions, such as Cu^{II} and Fe^{III}, are shown to overproduce reactive oxygen species (ROS) *via* Fenton-like reactions leading to oxidative stress.^[1b-d,3] Thus, it has been proposed that individual or inter-related reactivities of metal-free A β , metal ions, and ROS may contribute to AD pathogenesis [specially, *via* an inter-communicator, metal-bound A β (metal-A β)] (Figure 1).^[1c,1d,3d,3e]

To elucidate the molecular-level underpinnings of individual and inter-related risk features involved in AD pathogenesis, small molecules capable of targeting and modulating their reactivities have been developed as chemical tools.^[4] Among them, **L2-b** (*N*¹,*N*¹-dimethyl-*N*⁴-(pyridin-2-ylmethyl)benzene-1,4-diamine; Figure 1) was recently developed for regulating metal-A β species, along with antioxidant activity, and its *in vitro* and *in vivo* efficacy toward metal-A β was demonstrated.^[4b,4f] Until now, however, it has not been determined which and how the molecular formulas and properties of such the tool could lead to its reactivities specific for the desired target, which has restricted new or innovative tool development. Herein, we report our multidisciplinary studies employing a chemical library newly designed based on **L2-b**'s backbone (Figure 1) that demonstrate the importance of rationally constructing and tuning structural features and mechanisms (*e.g.*, peptide modifications, including degradation and covalent adduct formation, *via* oxidative transformations of small molecules based on their ionization potentials) toward development of tools for regulating distinct

- [a] Dr. Hyuck Jin Lee
School of Life Sciences
Ulsan National Institute of Science and Technology (UNIST)
Ulsan 44919 (Republic of Korea)
- [b] Dr. Kyle J. Korshavn, Dr. Richard A. Kerr, Prof. Dr. Brandon T. Ruotolo, Prof. Dr. Ayyalusamy Ramamoorthy
Department of Chemistry, University of Michigan
Ann Arbor, Michigan 48109 (USA)
E-mail: ramamoor@umich.edu (A. Ramamoorthy)
- [c] Younwoo Nam, Dr. Il Seung Youn, Juhye Kang, Prof. Dr. Kwang S. Kim and Prof. Dr. Mi Hee Lim
Department of Chemistry, UNIST
E-mail: mhlil@unist.ac.kr (M. H. Lim)
- [d] Thomas J. Paul, Dr. Mehmet Ozbil, Prof. Dr. Rajeev Prabhakar
Department of Chemistry, University of Miami
Coral Gables, Florida 33146 (USA)
E-mail: rpr@miami.edu (R. Prabhakar)
- [e] Prof. Dr. Ayyalusamy Ramamoorthy
Biophysics, University of Michigan

Supporting information for this article is given *via* a link at the end of the document.

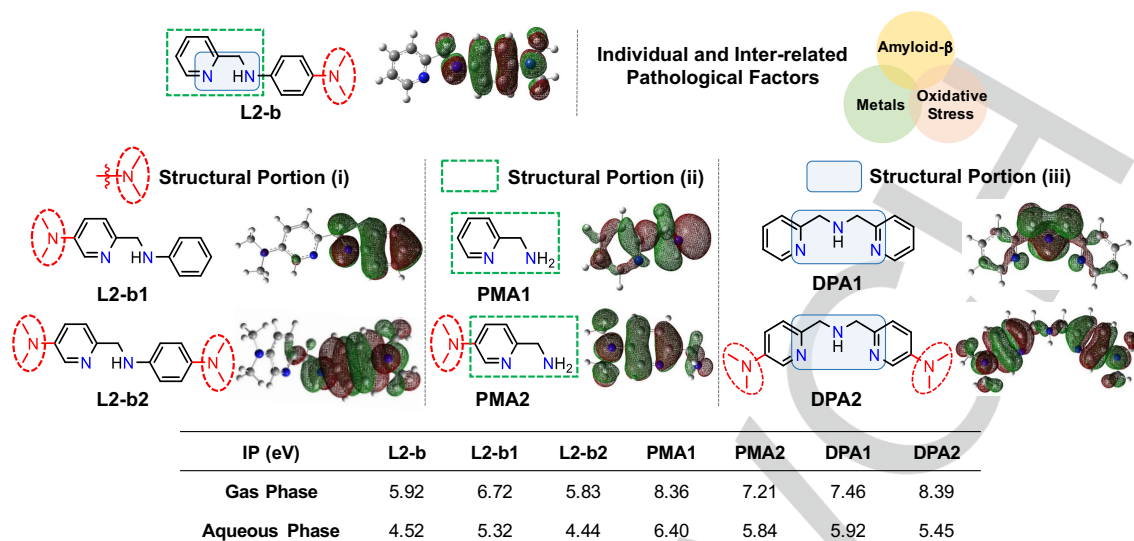


Figure 1. Structural investigations (i-iii) of small molecules to alter their ionization potentials (IPs) and reactivities with individual and inter-related AD pathological factors. Structural variations: (i) the different position and number of the dimethylamino functionality; (ii) the metal binding sites with and without a dimethylamino group; (iii) the increased denticity and structural flexibility. Potential donor atoms for metal binding are indicated in blue. Isosurface plots of compounds' SOMOs (blue, N; gray, C; white, H) are depicted underneath of compounds' structures. The calculated IPs in both the gas and aqueous phases are summarized in the table (bottom). **L2-b**, N^1,N^1 -dimethyl- N^2 -(pyridin-2-ylmethyl)benzene-1,4-diamine; **L2-b1**, N,N -dimethyl-6-((phenylamino)methyl)pyridin-3-amine; **L2-b2**, N^1 -((5-(dimethylamino)pyridin-2-yl)methyl)- N^4,N^4 -dimethylbenzene-1,4-diamine; **PMA1**, pyridin-2-yl-methanamine; **PMA2**, 6-(aminomethyl)- N,N -dimethylpyridin-3-amine; **DPA1**, bis(pyridin-2-ylmethyl)amine; **DPA2**, 6-((((5-(dimethyl-amino)pyridin-2-yl)methyl)amino)methyl)- N,N -dimethylpyridin-3-amine.

and inter-related pathological features in AD. Moreover, through the design principle gained from structural and mechanistic details, a chemical tool for targeting and controlling multiple distinguishable factors (i.e., metals, metal-free A β , metal-A β , and oxidative stress) was successfully constructed. Overall, our studies illustrate an instruction of how chemical tools can be devised for investigating individual or inter-related pathological factors in AD.

Results and Discussion

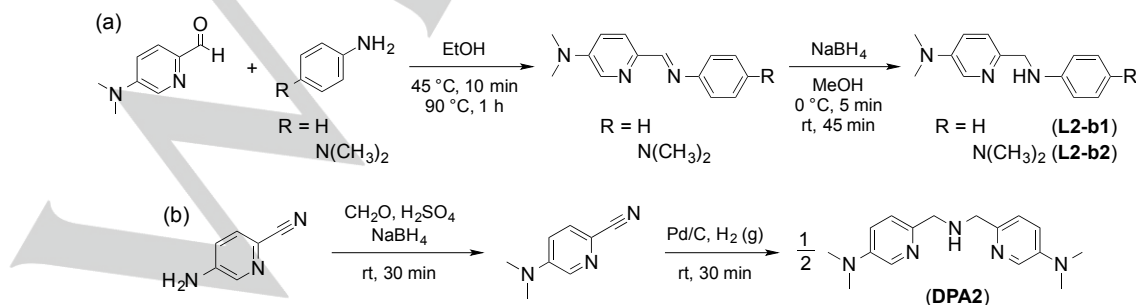
Rational selection and preparation of small molecules

In order to establish how structural characteristics can guide mechanistic directions of chemical tools for desired reactivities toward their distinct targets, a class of small molecules derived from the backbone of **L2-b** was rationally designed (Figure 1). In our chemical series, different structural variations or portions

based on the framework of **L2-b** were applied or selected (Figure 1): (i) the position and number of the dimethylamino functionality, important for A β interaction,^[4a-g,5] on the backbone of **L2-b** were altered affording **L2-b1** and **L2-b2**; (ii) the structural moieties of **L2-b** and **L2-b1/L2-b2** for metal binding (i.e., **PMA1** and **PMA2**, respectively) were included; (iii) the denticity and structural flexibility on **L2-b**'s structure were varied generating **DPA1** and **DPA2**. Moreover, the blood-brain barrier (BBB) permeability of our compounds was also considered for their biological applications. The potential BBB penetration of small molecules was suggested based on Lipinski's rules as well as the values obtained from logBB calculation and the Parallel Artificial Membrane Permeability Assay adapted for the BBB (PAMPA-BBB)^[4b,4c,4d,6] (Supporting Information, Table S1).

L2-b, **L2-b1**, **L2-b2**, and **DPA2** were prepared following the previously reported methods with slight modifications (especially for **L2-b1**, **L2-b2**, and **DPA2**, the procedures are summarized Scheme 1).^[4b,4d] **L2-b1** and **L2-b2** were obtained in a relatively

Scheme 1. Synthetic routes to (a) **L2-b1**, **L2-b2**, and (b) **DPA2**.



high yield through the formation of imine followed by its reduction to amine using sodium borohydride (NaBH_4).^[4b,4d] In the case of **DPA2**, the reduction of the primary amino group on picolinonitrile to the dimethylamino functionality was carried out subsequently incorporating themselves to obtain the final product. Note that **PMA1**, **PMA2**, and **DPA1** are commercially available.

Influence on metal-free and metal-induced $\text{A}\beta$ aggregation

The ability of our small molecules (Figure 1) to modulate $\text{A}\beta$ aggregation in both the absence and presence of metal ions was monitored through inhibition and disaggregation experiments (reaction schemes of both studies shown in Figure 2a and Supporting Information, Figure S1a, respectively). The experiments were performed using $\text{A}\beta_{40}$ and $\text{A}\beta_{42}$, two major $\text{A}\beta$ isoforms found in the AD-affected brain.^[1a-c] The molecular weight (MW) distributions and morphological changes of the resultant $\text{A}\beta$ species were analyzed by gel electrophoresis with Western blotting (gel/Western blot) and transmission electron microscopy (TEM), respectively.^[4a-h] If a compound could

generate a variety of smaller $\text{A}\beta$ species, the gel/Western blot would indicate significant smearing. The large aggregates produced upon treatment with a compound can be visualized by TEM, but are too large to penetrate into the gel matrix thus presenting very little smearing on the gel/Western blot (Figures 2, Supporting Information, Figure S1).

In inhibition experiments (analysis of compounds' effect on formation of $\text{A}\beta$ aggregates, Figure 2a), various MW distributions of both metal-free $\text{A}\beta_{40}$ and metal- $\text{A}\beta_{40}$ species were displayed to different extents from the samples containing **L2-b2** (lane 2, Figure 2b) compared to compound-untreated peptides (lane C, Figure 2b). On the other hand, much less significant influence on $\text{A}\beta$ aggregation was observed upon incubation with the other compounds (i.e., **L2-b1**, **PMA1**, **PMA2**, **DPA1**, and **DPA2**) with and without metal ions. Moreover, similar to $\text{A}\beta_{40}$, both metal-free and metal-treated $\text{A}\beta_{42}$ aggregation pathways were altered by treatment with **L2-b2** (lane 2, Figure 2c), noticeably different from **L2-b1**, **PMA1**, **PMA2**, **DPA1**, and **DPA2**. In addition to gel/Western blot analyses, the morphologies of both metal-free $\text{A}\beta_{40}/\text{A}\beta_{42}$ and metal- $\text{A}\beta_{40}/\text{A}\beta_{42}$ aggregates produced upon

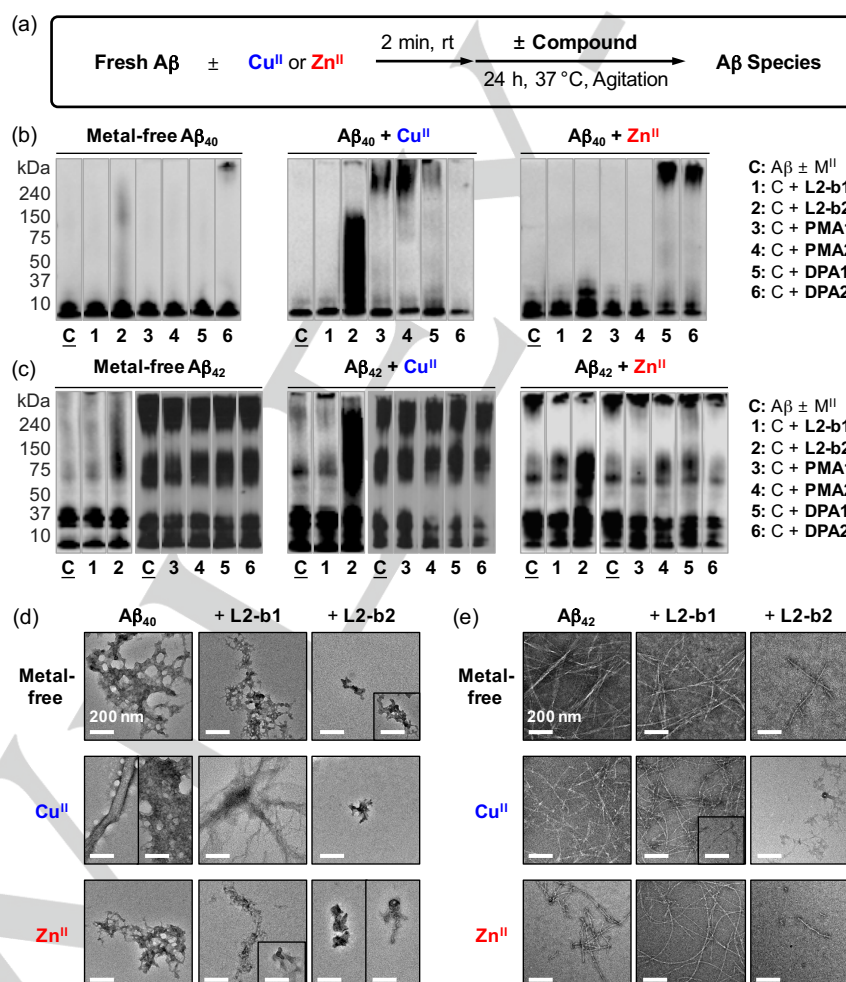


Figure 2. Effects of small molecules on formation of metal-free $\text{A}\beta$ and metal- $\text{A}\beta$ aggregates. (a) Scheme of the inhibition experiment. Visualization of MW distributions of resultant (b) $\text{A}\beta_{40}$ and (c) $\text{A}\beta_{42}$ species by gel/Western blot with an anti- $\text{A}\beta$ antibody (6E10). Conditions: $[\text{A}\beta] = 25 \mu\text{M}$; $[\text{CuCl}_2 \text{ or } \text{ZnCl}_2] = 25 \mu\text{M}$; $[\text{compound}] = 50 \mu\text{M}$; pH 6.6 (for Cu^{II} experiments) or pH 7.4 (for metal-free and Zn^{II} experiments); 37°C ; constant agitation. TEM images of the (d) $\text{A}\beta_{40}$ and (e) $\text{A}\beta_{42}$ samples from (b) and (c), respectively.

incubation with **L2-b1** or **L2-b2** were monitored by TEM. The resultant $A\beta_{40}$ and $A\beta_{42}$ aggregates generated by treatment with **L2-b2** were shown to be more amorphous aggregates and/or smaller fibrils than those obtained under compound-free and **L2-b1**-treated conditions (Figure 2d and 2e).

The results from disaggregation experiments (determination of the ability of compounds to disassemble preformed $A\beta$ aggregates; Supporting Information, Figure S1a) are similar to those from inhibition studies (Supporting Information, Figure S1b-e). Preformed metal-free $A\beta_{40}$ and metal-treated $A\beta_{40}$ aggregates incubated with **L2-b2** displayed various-sized peptide aggregates to different degrees (lane 2, Supporting Information, Figure S1b). Similar to inhibition experiments, **L2-b1**, **PMA1**, **PMA2**, **DPA1**, and **DPA2** could not detectably disaggregate preformed $A\beta_{40}$ aggregates or redirect their further aggregation under both metal-free and metal-present conditions (Supporting Information, Figure S1b). In the case of $A\beta_{42}$, **L2-b2** was also indicated to dismantle preformed metal-free and metal-treated $A\beta_{42}$ aggregates, distinct from the other compounds (Supporting Information, Figure S1c). Expected from the gel/Western blot studies, more noticeable morphological changes upon treatment of **L2-b2** to preformed metal-free and metal-bound $A\beta_{40}/A\beta_{42}$ aggregates were visualized, indicating more amorphous aggregates or thinner fibrils than the resultant $A\beta$ aggregates from compound-free and **L2-b1**-added samples (Supporting Information, Figure S1d and S1e).

Collectively, our gel/Western blot and TEM results suggest that structural variations of small molecules govern their distinct reactivities toward both metal-free and metal-induced $A\beta$ aggregation. **L2-b2**, which has the overall structure of **L2-b** with an additional dimethylamino group on the pyridine ring (Figure 1), is observed to redirect both metal-free $A\beta$ and metal- $A\beta$ aggregation pathways; however, **L2-b1** with the dimethylamino functionality, differently positioned from the backbone of **L2-b**, is not able to alter peptide aggregation regardless of the presence of metal ions. **PMA1** and **PMA2**, the metal chelating portions of **L2-b** and **L2-b1/L2-b2**, respectively (Figure 1), could not significantly control $A\beta$ aggregation in both the absence and presence of metal ions. In addition, **DPA1** and **DPA2** (Figure 1), the small molecules with the greater metal binding denticity and structural flexibility than **L2-b**, are not capable of distinguishably impacting $A\beta$ aggregation even in the presence of metal ions. Therefore, the results and observations from both the inhibition and disaggregation studies employing our chemical series validate that the overall framework of **L2-b** with the dimethylamino group(s) at proper position(s), instead of individual structural components, could achieve inhibitory reactivities of small molecules with metal-free $A\beta$ and/or metal- $A\beta$.

Biological activities

The capability of each compound to mediate cytotoxicity triggered by metal ions, metal-free $A\beta$, and metal- $A\beta$ was examined. More than ca. 85% of cell survival was exhibited when **L2-b1**, **L2-b2**, **PMA1**, **PMA2**, **DPA1**, and **DPA2** (up to 50 μ M without metal ions; up to 25 μ M with metal ions) were treated

to human neuroblastoma SK-N-BE(2)-M17 (M17) cells (Supporting Information, Figure S2). Additionally, the regulating activity of **L2-b2**, able to noticeably control both metal-free and metal-treated $A\beta$ aggregation (*vide supra*), against cytotoxicity induced by metal-free $A\beta$ or metal- $A\beta$ was further verified (Figure 3a). As shown in Figure 3a, our molecules in this study have relatively low toxicity in both the absence and presence of metal ions under conditions tested. Moreover, **L2-b2**, which has an additional dimethylamino group on **L2-b**'s backbone, is observed to possibly alleviate toxicity triggered by metal-free $A\beta$ and metal- $A\beta$ in living cells due to its abilities to modulate $A\beta$ aggregation (*vide supra*) and scavenge free radicals (*vide infra*).

The capability of **L2-b1**, **L2-b2**, **PMA1**, **PMA2**, **DPA1**, and **DPA2** to scavenge free radicals was measured by the Trolox (vitamin E analogue) equivalent antioxidant capacity (TEAC) assay which can evaluate compounds' capability of quenching ABTS cation radicals [$ABTS^{+}$; $ABTS = 2,2'$ -azino-bis(3-ethylbenzothiazoline-6-sulfonic acid)] in both an organic solution (*i.e.*, EtOH) and a biologically relevant environment (*i.e.*, cell lysates).^[4c-g,7] As shown in Figure 3b, the TEAC values of **L2-b1** and **L2-b2** [0.8 (\pm 0.1) and 1.9 (\pm 0.1) in EtOH; 0.7 (\pm 0.1) and 1.1 (\pm 0.1) in M17 lysates, respectively] were determined. The compound **L2-b2** presents a greater ability to quench free organic radicals than Trolox in both media, EtOH and cell lysates. The noticeable free organic radical scavenging ability of **L2-b1** and **L2-b2**, compared to **PMA1**, **PMA2**, **DPA1**, and **DPA2**

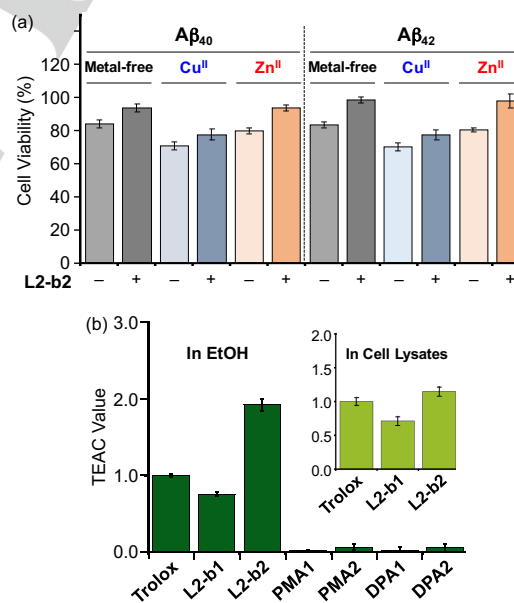


Figure 3. Biological activities of small molecules. (a) Viability of cells treated with **L2-b2** and $A\beta_{40}$ or $A\beta_{42}$ in the absence and presence of $CuCl_2$ or $ZnCl_2$. SK-N-BE(2)-M17 (M17) cells were incubated with metal-free $A\beta$ and metal- $A\beta$ followed by the addition of **L2-b2**. Cell viability (%) was determined by the MTT assay compared to cells treated with DMSO only (0–1%, v/v). Conditions: $[A\beta] = 10 \mu$ M; $[CuCl_2]$ or $[ZnCl_2] = 10 \mu$ M; $[L2-b2] = 20 \mu$ M. (b) Free organic radical scavenging capability of **L2-b1**, **L2-b2**, **PMA1**, **PMA2**, **DPA1**, and **DPA2**, identified by the TEAC assay in EtOH or M17 cell lysates (inset). The TEAC values are relative to that of a vitamin E analogue, Trolox (6-hydroxy-2,5,7,8-tetramethylchroman-2-carboxylic acid). Error bars represent the standard error (SE) from three independent experiments ($P < 0.05$).

is expected from their relative lower IP values (*vide infra*, Figure 1). Together, the entire framework of **L2-b** (with and without additional dimethylamino group(s)) over individual structural portions is responsible for relative lower IP values that could offer the distinct scavenging activity of small molecules toward free radicals.

Mechanisms for modulating reactivities toward metal-free and metal-bound A β species

(i) Ionization potentials. The IPs of our small molecules (Figure 1) were calculated to anticipate the possibility of their modulating ability toward A β aggregation pathways and antioxidant capability. As depicted in Figure 1, **L2-b** and **L2-b2** are shown to have relatively lower IP values than the other structures (*i.e.*, **L2-b1**, **PMA1**, **PMA2**, **DPA1**, and **DPA2**) in both the gas and aqueous phases. Moreover, the singly occupied molecular orbitals (SOMOs) indicate that the structures of **L2-b** and **L2-b2**, composed of a dimethylamino group on the benzene ring, are observed to be more easily oxidized than that the structure with the dimethylamino functionality only on the pyridine ring (*i.e.*, **L2-b1**). Based on the IP values of our chemical series, oxidative transformations of the compounds (particularly, **L2-b** and **L2-b2**) could occur and subsequently direct their regulatory ability against A β peptides and free radicals (*vide supra*).

(ii) Metal binding. Cu^{II} or Zn^{II} binding of compounds was monitored by UV-vis or ¹H nuclear magnetic resonance (NMR) spectroscopy. Changes of the UV-vis spectra were observed

upon addition of CuCl₂ to the EtOH solution of all small molecules (Figure 1), indicative of their binding to Cu^{II} (Supporting Information, Figure S3a-f). In case of **L2-b1** and **L2-b2**, new optical bands were detected; for **PMA1** and **DPA1**, the intensity of the absorption spectra was increased; the spectral shifts of **PMA2** and **DPA2** were observed upon treatment with Cu^{II} (Supporting Information, Figure S3a-f). Furthermore, Zn^{II} binding of compounds was investigated by UV-vis and ¹H NMR. The addition of Zn^{II} (1 equiv) to the CD₃CN solution of **L2-b1**, **PMA1**, or **PMA2** caused the variation of chemical shifts of the pyridyl protons suggesting the involvement of the N donor atoms on their pyridine ring in Zn^{II} binding (Supporting Information, Figure S3g-i). In addition, the optical spectra of **L2-b2**, **DPA1**, and **DPA2** were altered upon introduction of Zn^{II} to their EtOH solution (Supporting Information, Figure S3j-l). Together, our UV-vis and NMR studies present that our molecules can interact with Cu^{II} and Zn^{II}.

(iii) Interactions with metal-free and Zn^{II}-treated A β ₄₀ monomers. **L2-b2** is indicated to have its modulating ability toward both metal-free A β and metal-A β aggregation pathways, distinct from the other small molecules [particularly, **L2-b** (reactivity only for metal-A β species)^[4b,4f] and **L2-b1** (no noticeable reactivity for both metal-free A β and metal-A β); Figure 2 and Supporting Information, Figure S1]. In order to pinpoint the different reactivity of these small molecules (*i.e.*, **L2-b**, **L2-b1**, **L2-b2**) toward targets, the interactions of **L2-b1** and **L2-b2** with monomeric A β ₄₀ in the absence of metal ions were

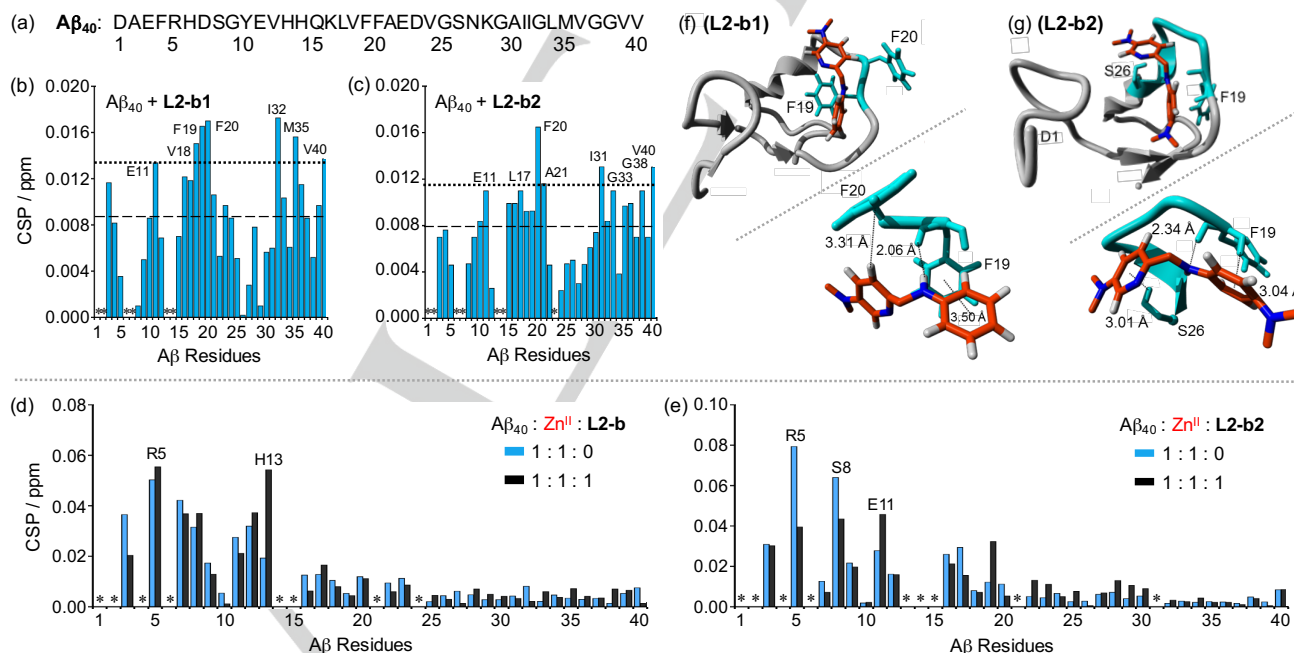


Figure 4. Interactions of **L2-b**, **L2-b1**, or **L2-b2** with metal-free or Zn^{II}-treated A β ₄₀ monomer. (a) Amino acid sequence of A β ₄₀. Plots of the chemical shift perturbation (CSP) determined through 2D ¹H-¹⁵N SOFAST-HMQC NMR spectra of uniformly ¹⁵N-labeled monomeric A β ₄₀ upon titration with (b) **L2-b1** or (c) **L2-b2**. The average CSP (dashed line) with standard deviation (dotted line) is presented. *Residues could not be resolved for analysis. Conditions: [A β ₄₀] = 80 μ M; [L2-b1 or L2-b2] = 0 or 800 μ M; 20 mM PO₄, pH 7.4, 50 mM NaCl; 7% D₂O (v/v); 10 °C. Plots of the CSP obtained from 2D ¹H-¹⁵N SOFAST-HMQC NMR spectra of uniformly ¹⁵N-labeled monomeric A β ₄₀ upon addition of Zn^{II} without (blue) and with (black) (d) **L2-b** or (e) **L2-b2**. *Residues could not be resolved for analysis. Conditions: [A β ₄₀] = 80 μ M; [ZnCl₂] = 80 μ M; [L2-b or L2-b2] = 80 μ M; 20 mM PO₄, pH 7.4, 50 mM NaCl; 7% v/v D₂O. MD simulations showing interactions of (f) **L2-b1** or (g) **L2-b2** with monomeric A β ₄₀. Possible sites and energy of interactions of A β ₄₀ (PDB 1BA4) with **L2-b1** or **L2-b2** after all-atom MD simulations are summarized. The zoomed-in view (right, below) of each binding site with residues showing interaction distances labelled in Å with dashed lines (additional MD simulations data in Supporting Information, Figure S5).

first investigated by 2D band-selective optimized flip-angle short transient heteronuclear multiple quantum correlation (SOFAST-HMQC) NMR spectroscopy (Figure 4b, 4c and Supporting Information, Figure S4). Small but detectable chemical shifts were presented upon titration with 10 equiv of the compounds to metal-free A β ₄₀ monomer (Supporting Information, Figure S4). To identify the amino acid residues potentially involved in binding of compounds to the peptide, their chemical shift perturbation (CSP) was calculated (Figure 4b and 4c) indicating that **L2-b1** and **L2-b2** triggered slightly noticeable CSP at the residues [E11; L17-A21 (the self-recognition);^[1c,1d] I31-G33, M35, G38, and V40 at the hydrophobic C-terminal region] to different degrees, relatively similar to **L2-b**.^[4e] **L2-b1** and **L2-b2** resulted in the chemical shift of V40 at the C-terminus, like **L2-b**,^[4e] which may reflect the rearrangement of the disordered C-terminus to pack against the compounds instead of direct or indirect interactions with A β ₄₀. Overall, the compounds (*i.e.*, **L2-b1**, **L2-b2**, and **L2-b**^[4e]) are observed to have weak interactions with metal-free A β .

To visualize the interactions between **L2-b**, **L2-b1**, or **L2-b2** and monomeric A β ₄₀ (PDB 1BA4),^[8] studies *via* molecular docking and molecular dynamics (MD) simulations were conducted. Both rigid and flexible docking procedures were utilized using the Autodock Vina 1.5.6 program.^[9] MD simulations were performed on the starting structure obtained from docking procedures on complexes of **L2-b**, **L2-b1**, or **L2-b2** with A β ₄₀. These all-atom simulations were run by the GROMOS96 53a6 force field as implemented in the GROMACS program.^[10] Multiple interactions of compounds with A β ₄₀ (*i.e.*, π - π interaction, C-H- π interaction, N-H- π interaction, hydrogen bonding) were observed (Figure 4f, 4g and Supporting Information, Figure S5). First, **L2-b** may interact with both polar and non-polar residues through hydrogen bonding between its secondary amine and H6 and π - π interactions between its benzene/pyridine rings and F4 or H14, respectively (Supporting Information, Figure S5a; left). Other amino acid residues of A β ₄₀ (*e.g.*, L17 and F19) were also shown to be involved in interactions with **L2-b** through hydrogen bonding and a π - π interaction, respectively (Supporting Information, Figure S5a; right). As shown in Figure 4f, **L2-b1** was held between two aromatic residues, F19 and F20, through π - π and C-H interactions, respectively. Additionally, hydrogen bonding between the backbone carbonyl O atom (between F19 and F20) and **L2-b1**'s secondary amine bridging the two aromatic rings could be generated. Three aromatic residues H6, Y10, and H14 might interact with **L2-b1** through a π - π interaction (Y10), a C-H- π interaction (H14), and hydrogen bonding (H6 and D7) (Supporting Information, Figure S5b; right).

The residues F19 and S26 were indicated to interact with **L2-b2** through C-H- π interactions (between **L2-b2**'s benzene ring and the H atom from the aromatic ring of F19; between **L2-b2**'s pyridine ring and the H atom from ¹³C of S26) (Figure 4g). Additionally, **L2-b2**'s secondary amine group and the backbone carbonyl O atom between F19 and F20 may form hydrogen bonding. Moreover, **L2-b2** could be held between two aromatic residues F4 and F20 *via* C-H- π (between its pyridine ring and

the H atom from the aromatic ring of F4) and N-H- π (between its secondary amine and F20) interactions, respectively. Hydrogen bonding between the N atom of dimethylamino group on **L2-b2**'s benzene ring and the backbone amine group of S8 could also be formed (Supporting Information, Figure S5c; right). For all binding modes, binding energies and contributions of electrostatic or hydrophobic interactions were calculated and summarized in the table (Supporting Information, Figure S5). Together, through MD simulations, the potential interactions of **L2-b**, **L2-b1**, and **L2-b2** with metal-free A β ₄₀ monomer could be envisioned. Based on our 2D NMR, MS, and MD simulations studies, the regulatory activity of molecules with metal-free A β may be achieved *via* the covalent adduct formation (observed by **L2-b2**; Figure 5b) rather than non-covalent interactions (*e.g.*, π - π and C-H- π interactions, hydrogen bonding).

The interaction of monomeric A β ₄₀ with **L2-b2** capable of controlling metal-free A β aggregation (*vide supra*; Figure 2 and Supporting Information, Figure S1) was further monitored by electrospray ionization mass spectrometry (ESI-MS) (Figure 5a, 5b and Supporting Information, Figure S6). Different from **L2-b** unable to interact with metal-free A β ,^[4b,4f] **L2-b2** or its degraded compounds [*e.g.*, *N,N*-dimethyl-*p*-phenylenediamine (**DMPD**) and/or oxidized **DMPD** (*i.e.*, cationic imine, **CI**)^[4g] were shown to have interactions with metal-free A β (Figure 5b). When **L2-b2** was incubated with metal-free A β , a newly observed signal corresponding to the addition of 132 Da to A β , indicative of forming a covalent adduct of **CI**-A β , was exhibited (magenta, Figure 5b). This adduct could be generated *via* primary amine-containing residues from A β (*e.g.*, K16, K28) (Figure 5b and Supporting Information, Figure S6), similar to the complex formation of benzoquinone (**BQ**) with A β (**BQ**-A β)^[4g] Such distinct interactions of **L2-b2** with A β (*i.e.*, the compounds' degradation and transformation followed by covalent cross-links with A β) could be associated with **L2-b2**-triggered alteration of metal-free A β aggregation, which was not observed from the samples of A β with **L2-b**.^[4f]

For the interaction with Zn^{II}-A β , 2D NMR was employed to analyze the samples containing **L2-b** or **L2-b2** and Zn^{II}-bound uniformly ¹⁵N-labeled A β ₄₀ monomer (Figure 4d, 4e and Supporting Information, Figure S7). **L2-b** induced relatively more CSP of R5 and H13 residues close to a metal binding site of A β ₄₀ (Figure 4d).^[1b-d,3d,3e] As shown in Figure 4e, similar to **L2-b**, **L2-b2** caused CSP of residues, such as R5, S8, and E11, within proximity of the metal binding region. Thus, **L2-b** and **L2-b2** could interact with Zn^{II} surrounded by A β ₄₀ possibly leading to mediation of Zn^{II}-A β ₄₀ aggregation, as detected by gel/Western blot and TEM (Figure 2 and Supporting Information, Figure S1).

(iv) Interactions with metal-free and Zn^{II}-treated A β fibrils.

Along with A β monomer, to verify how **L2-b** or **L2-b2** is able to disassemble preformed metal-free and/or metal-added A β aggregates to different extents, their interactions with metal-free and Zn^{II}-treated A β ₄₂ fibrils were studied by saturation transfer difference (STD) NMR (Figure 6a-c). Signals in STD NMR are proportional to each atom of either **L2-b** or **L2-b2** to its macromolecular binding partner, fibrils, which allows atomic-level mapping of ligand binding to fibrillar A β .^[11] In the case of

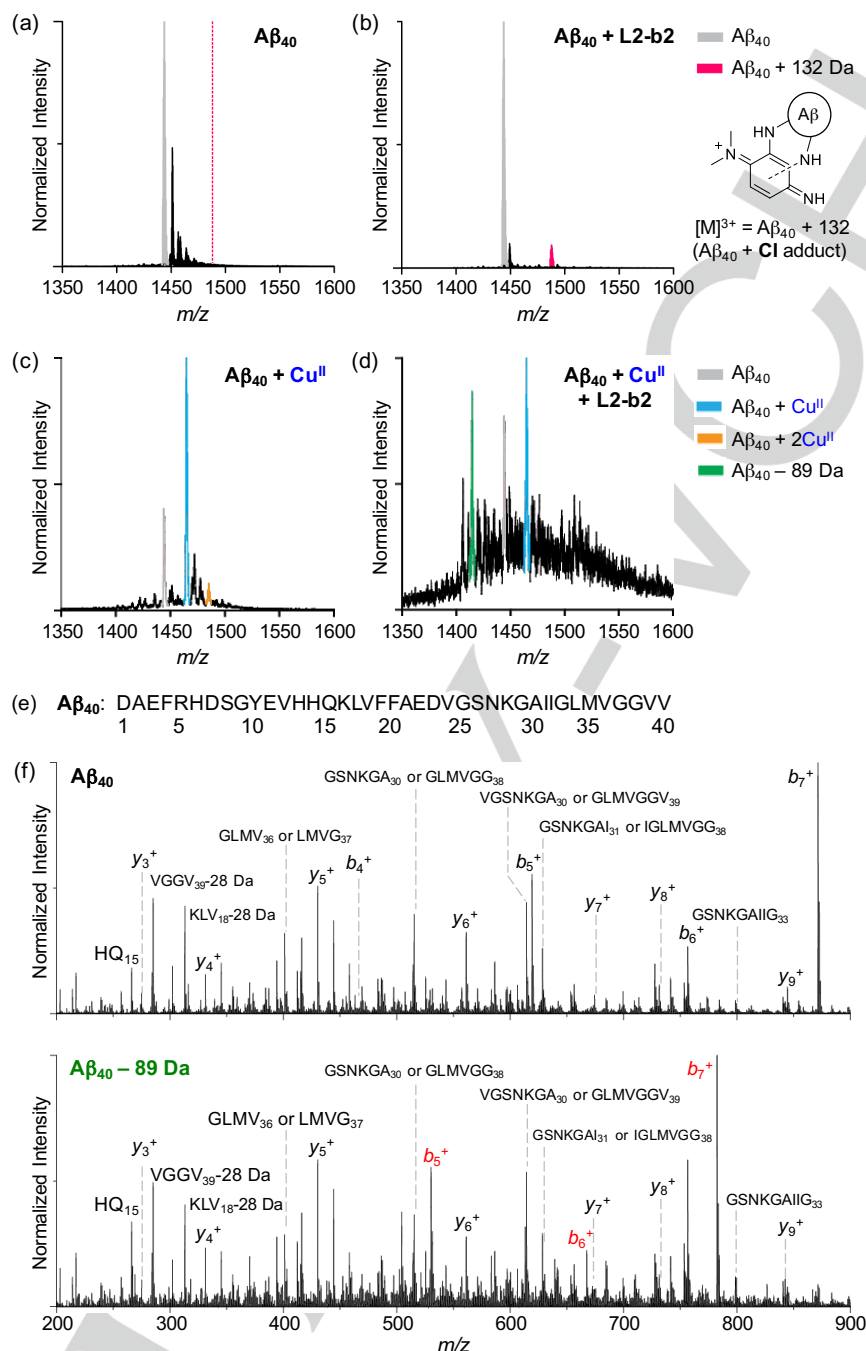


Figure 5. ESI-MS analysis of Aβ₄₀ incubated with L2-b2 in the absence and presence of Cu^{II}. (a and b) The 3+ charge state of metal-free Aβ₄₀ with and without L2-b2. When L2-b2 was treated with Aβ, the signal at *m/z* 1487.8 (131.97 Da increase from Aβ₄₀) possibly corresponding to an adduct formed with Aβ and oxidized DMPD (CI; cleaved from L2-b2) was observed. Conditions: [Aβ₄₀] = 10 μM; [CuCl₂] = 10 μM; [L2-b2] = 50 μM; 20 mM ammonium acetate, pH 7.5; 37 °C; 6 h incubation; no agitation. The 3+ charge state of Aβ₄₀ incubated with (c) Cu^{II} or (d) both Cu^{II} and L2-b2. The signal highlighted in green corresponds to degraded Aβ by loss of 89.08 Da. Conditions: [Aβ₄₀] = 20 μM; [CuCl₂] = 20 μM; [L2-b2] = 120 μM; 100 mM ammonium acetate, pH 7.5; 37 °C; 30 min incubation; no agitation. (e) Amino acid sequence of Aβ₄₀. (f) MS/MS analyses of Aβ₄₀ with and without treatment of Cu^{II} and L2-b2. These data support that the amino acid sequence of Aβ is chemically modified within the first five residues (D₁A₂E₃F₄R₅) of the peptide in the presence of both Cu^{II} and L2-b2. All the Aβ₄₀ species containing the identified -89.08 Da covalent modification are highlighted in red, and are compared against control Aβ₄₀ MS/MS sequencing data acquired under the same conditions.

L2-b, the relatively strong saturation effect was observed at the pyridine ring with metal-free Aβ₄₂ fibrils with the slight saturation effect at the dimethylamino group. In addition to the pyridine ring, upon treatment of Zn^{II}-Aβ fibrils with L2-b, the relatively

noticeable saturation effects on the molecule were also indicated at the methyl group between the pyridine ring and the secondary amine (Figure 6c; left). Different from L2-b, both two dimethylamino groups and the pyridine ring of L2-b2 were

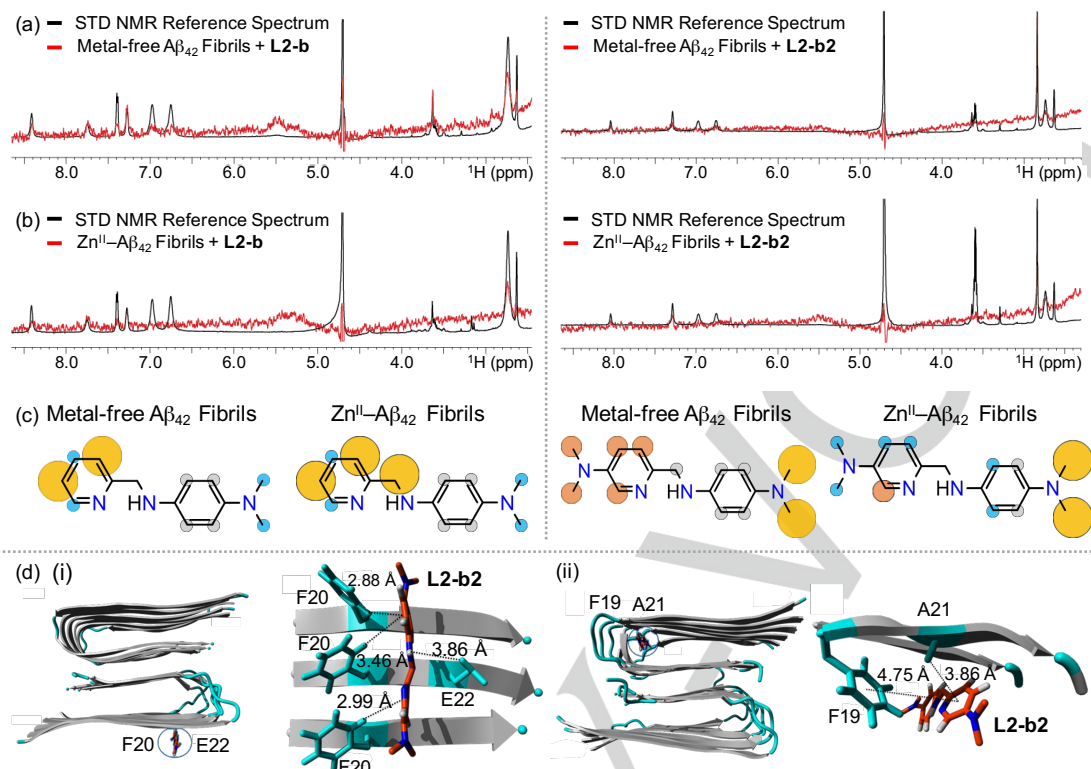


Figure 6. Interactions of **L2-b** or **L2-b2** with metal-free and Zn^{II}-treated Aβ₄₂ fibrils. ¹H STD NMR spectra of **L2-b** (left) or **L2-b2** (right) in the presence (red) and absence (black) of (a) metal-free or (b) Zn^{II}-treated Aβ₄₂ fibrils. Comparison of the STD signal intensities (red) to the STD reference (black) reflects the relative proximity of the corresponding proton from the ligand to Aβ₄₂ fibrils. Conditions: [Aβ₄₂] = 2 μM; [ZnCl₂] = 2 μM; [**L2-b** or **L2-b2**] = 200 μM; 10 mM Tris-DCl, pH 7.4. (c) Normalized STD intensities mapped on to the structures of **L2-b** and **L2-b2** against metal-free Aβ₄₂ fibrils (left) and Zn^{II}-Aβ₄₂ fibrils (right). Yellow, orange, and blue circles indicate the STD effects of > 75%, 50–75%, and < 50%, respectively. Gray circles indicate the absence of the STD effect. (d) MD simulations showing interactions of **L2-b2** with metal-free Aβ₄₀ fibrils. Two potential binding sites (i and ii) of interaction of **L2-b2** with Aβ₄₀ fibrils (PDB 2LMN) after all-atom MD simulations. Right: The zoomed-in view of each binding site with residues showing interaction distances labelled in Å with dashed lines. Binding modes (for **L2-b**) and energies (for both **L2-b** and **L2-b2**) are presented in Supporting Information, Figure S8.

presented to have relatively significant saturation effects against metal-free Aβ₄₂ fibrils (Figure 6c; right), suggesting that this molecule could be relatively packed into the fibrillar conformation of Aβ, as described by a previously reported compound.^[4d] When Zn^{II} was introduced to Aβ₄₂ fibrils, the saturation effects on the dimethylamino group of the pyridine ring was observed to be relatively less than those on that of the benzene ring, along with the reduced saturation influence on the pyridine ring.

To gain a better understanding of the interactions between Aβ fibrils (PDB 2LMN)^[12] and **L2-b** or **L2-b2**, MD simulations were further conducted. As shown in Figure 6d and Supporting Information, Figure S8, two binding modes (*i.e.*, for both **L2-b** and **L2-b2**, alignment orthogonal to the surface of the β-strand; for **L2-b2**, intercalation into the loop of two β-strands) were observed. The complex of **L2-b** and fibrillar Aβ₄₀ formed hydrogen bonding of the H atoms from the benzene ring, the pyridine ring, and the secondary amine bridging two aromatic rings of **L2-b** with the O atoms from the carboxyl groups of E22s, as well as the N atom from the pyridine ring of **L2-b** with the H atom from aromatic ring of F20 (Supporting Information, Figure S8a). Additionally, a C–H–π interaction (between the H atom from the benzene ring of **L2-b** and the aromatic ring of F20) could stabilize the molecule to interact with Aβ fibrils (Supporting

Information, Figure S8a). In the case of **L2-b2**, this small molecule could be held on the fibril edge of the β-strand through a C–H–π interaction with F20 (between the pyridine/benzene rings of **L2-b2** and the H atoms from the aromatic rings of F20s). E22 may further assist in **L2-b2** binding to Aβ fibrils through hydrogen bonding formation between the H atom from the secondary amine between two aromatic rings of **L2-b2** and the O atom from the carbonyl group of E22 (Figure 6d(ii)). Furthermore, **L2-b2** could be packed within the hydrophobic pocket of the fibril (intercalation into the loop of two β-strands) utilizing the interactions with A21 and F19 [C–H–π (between the pyridine ring of **L2-b2** and the H atom from the methyl group of A21) and π–π (between the pyridine ring of **L2-b2** and the aromatic ring of F19) interactions] (Figure 6d(ii)). This binding mode (packed by fibrils; intercalation) at the hydrophobic pocket, expected from STD NMR results (*vide supra*), may be linked to the relatively stronger direct interaction of **L2-b2** with preformed metal-free Aβ aggregates, as shown in a previously reported compound.^[4d]

Taken together, STD NMR and MD simulations suggest how **L2-b** and **L2-b2** could interact with metal-free Aβ fibrils and Zn^{II}-Aβ fibrils. Through STD NMR, the metal binding portion of **L2-b** (**PMA1**; Figure 1) was observed to be related to the contact with

Zn^{II}-A β fibrils. In addition, different structural portions of **L2-b2** are indicated to have noticeable interactions with metal-free A β fibrils and Zn^{II}-A β fibrils. Furthermore, MD simulations visualize how such structural features of **L2-b** and **L2-b2** interact with A β fibrils, which suggests compounds' binding modes against peptide fibrils (especially, for **L2-b2**, alignment on the surface of the β -strand and intercalation into the loop that connects the two β -strands). Thus, the structural difference between **L2-b** and **L2-b2** (*i.e.*, additional dimethylamino group) is indicated to distinctly interact with metal-free and Zn^{II}-treated A β fibrils.

(v) Generation of degraded A β . In order to determine how **L2-b2** is able to alter Cu^{II}-A β aggregation, nano-ESI-MS (nESI-MS) optimized for the detection of non-covalent protein complexes was applied.^[13] When the peptide was incubated with **L2-b2** in the presence of Cu^{II}, additional *m/z* signals corresponding to a mass loss of 89.08 (\pm 0.06) Da compared to apo A β_{40} were detected (green signal, Figure 5d), similar to the results of **L2-b**.^[4f] Tandem MS (MS/MS) sequencing indicates that this signal represents a modified form of A β_{40} which lacks 89.08 Da from the first five residues of the N-terminus (D₁A₂E₃F₄R₅) (Figure 5e and 5f). These MS/MS data indicate that **L2-b2** likely binds to A β proximal to the binding site of Cu^{II}.^[1b-d,3d,3e] Neither **L2-b2** nor Cu^{II} was directly detected in the complex with either the N-terminal cleavage product or apo A β_{40} supporting the formation of a transient ternary complex consistent with previously published results.^[4f] These data support that, compared to **L2-b**,^[4f] the additional dimethylamino functionality on the pyridine ring is shown to still generate N-terminally cleaved A β species (loss of 89.08 Da) that could redirect Cu^{II}-A β aggregation. Along with the MS data (Figure 5d and 5f), compared to **L2-b**, these observations suggest that the additional dimethylamino moiety enables the compound (*i.e.*, **L2-b2**) to interact and react with both metal-free and Cu^{II}-bound A β .

(vi) Proposed mechanisms for reactivities of L2-b2 toward metal-free A β and metal-A β . Multiple mechanisms of **L2-b2** to redirect A β aggregation in the absence and presence of metal ions are proposed on the basis of our NMR, MS, and computational results. **L2-b2** could be cleaved through oxidative and hydrolytic processes generating transformed **DMPD** (**DMPD**_{transformed})^[4g] that can be covalently bound to A β monomers to form an **DMPD**_{transformed}-A β (**CI-A β** ; Figure 5b) adduct. Upon **CI-A β** adduct formation, metal-free A β aggregation pathways could be redirected as previously reported.^[4f] In addition, as shown in Figure 6, **L2-b2** could be intercalated between β -sheets of A β fibrils, which could be associated with its regulatory activity with metal-free A β fibrils, possibly similar to a previously reported molecule.^[4d] In the presence of Zn^{II}, **L2-b2** is indicated to interact with monomeric A β (close to the metal binding site of A β)^[1b-d,3d,3e] (Figure 4), which implies its potential contact with Zn^{II} surrounded by A β subsequently modulating peptide aggregation. More detailed studies of **L2-b2**'s interaction with Zn^{II}-A β are the subject of future studies. Lastly, toward Cu^{II}-A β , **L2-b2** is able to lead to A β degradation (Figure 5), similar to **L2-b**.^[4f] This observed A β degradation could be related to the formation of a transient ternary complex between A β , Cu^{II}, and **L2-b2**, subsequently followed by **L2-b2**'s oxidation and A β degradation of by well-

known radical-mediated pathways.^[14] Such degraded A β could lose aggregation propensity as full-length peptides.^[4f] Based on analyses of A β products from both reactions of **L2-b2** with metal-free A β and Cu^{II}-A β , the oxidation of this molecule occurs, which suggests that its oxidative transformation is required for the desired reactivities with an emphasis on importance of anticipating IP values for rational design (Figure 1). Collectively, **L2-b2** is demonstrated to be a tool able to interact and react with all metal-free A β , Cu^{II}-A β , and Zn^{II}-A β to different extents *via* several disparate mechanisms.

Conclusions

Chemical tools capable of targeting and controlling individual or multiple pathogenic factors found in AD have been developed to elucidate AD pathogenesis at the molecular level; however, such tool invention has been challenging. Unfortunately, a guideline of designing chemical tools for distinct targets (*e.g.*, as the first step, selecting key structural and mechanistic properties of tools) has not been established. To contribute to this foundation, a new class of small molecules was constructed based on the structure of **L2-b**, known as a chemical regulator for metal-A β ,^[4b,4f] with consideration of their BBB permeability and relatively low cytotoxicity. Employing our chemical series, the regulatory activities toward metal-free A β and metal-A β aggregation, along with free radical scavenging capability, are observed to be directed by compounds' structures (*e.g.*, functionality and entire backbone) as well as mechanistic characteristics (*e.g.*, covalent adduct formation with peptides and peptide degradation through compounds' transformations). Through our structure-mechanism-based design, a molecular multifunctional tool, **L2-b2**, was newly fashioned showing its abilities to regulate all of our desired targets (*i.e.*, metals, metal-free A β , metal-A β , oxidative stress). Taken together, our overall multidisciplinary studies through a chemical library present a design concept of chemical tools toward individual or multiple inter-related pathological factors in AD based on structural and mechanistic details. Our structure-mechanism-based concept could open new avenues for devising chemical tools capable of regulating the actions of diverse pathological factors in human diseases. In principle, depending on different targets, distinct mechanisms of chemical tools to regulate their actions should be taken into account.

Experimental Section

Materials and methods

All reagents and solvents were purchased from commercial suppliers and used as received unless otherwise stated. **PMA1**, **PMA2**, and **DPA1** were purchased from Sigma-Aldrich (St. Louis, MO, USA). **L2-b**, **L2-b1**, **L2-b2**, and **DPA2** were synthesized as previously reported procedures (*vide infra*).^[4b] A β_{40} and A β_{42} were purchased from AnaSpec (Fremont, CA, USA) (A β_{42} = DAEFRHDSGYEVHHQKLVFFAEDVGSNKGAIIGLMVGGVVIA). Double distilled H₂O (ddH₂O) was obtained from a Milli-Q Direct 16 system (Merck KGaA, Darmstadt, Germany). An Agilent 8453 UV-visible (UV-vis) spectrophotometer (Santa Clara, CA, USA) was

used to measure optical spectra. TEM images were taken using a JEOL JEM-2100 transmission electron microscope (UNIST Central Research Facilities, Ulsan, Republic of Korea). Absorbance values for biological assays, including the MTT and TEAC assays, were measured on a SpectraMax M5e microplate reader (Molecular Devices, Sunnyvale, CA, USA). NMR studies of A β with compounds in both the absence and presence of Zn^{II} were carried out on a 900 MHz Bruker spectrometer equipped with a cryogenic probe (Michigan State University in Lansing, MI, USA). A Waters (Milford, MA) Synapt G2 HDMS equipped with a nano-electrospray ionization (nESI) or ESI source (Waters, Milford, MA, USA) was used to study complex formation between L2-b2 and A β ₄₀ with and without Cu^{II}.

Acknowledgements

This work was supported by the National Research Foundation (NRF) of Korea grant funded by the Korean government [NRF-2014R1A2A2A01004877 and 2016R1A5A1009405 (to M.H.L.); NRF-2014S1A2A2028270 (to M.H.L. and A.R.)]; the 2016 Research Fund (Project Number 1.160001.01) of Ulsan National Institute of Science and Technology (UNIST) (to M.H.L.); the University of Michigan Protein Folding Disease Initiative (to A.R., B.T.R., and M.H.L.); an NIH grant (to A.R.); the James and Esther King Biomedical Research Program of the Florida State Health Department Award [DOH grant number 08KN-11 to R.P.]; the National Honor Scientist Program (2010-0020414) of NRF of Korea (to K.S.K.). J.K. thanks the support from the Global Ph.D. fellowship program through the National Research Foundation of Korea (NRF) funded by the Ministry of Education (NRF-2015H1A2A1030823). We thank Drs. Michael Beck, Shin Jung Lee, and Woo Jong Cho for valuable comments about L2-b, ESI-MS analysis, and IP calculations, respectively.

Keywords: Amyloid- β • metal ions • oxidative stress • chemical tools

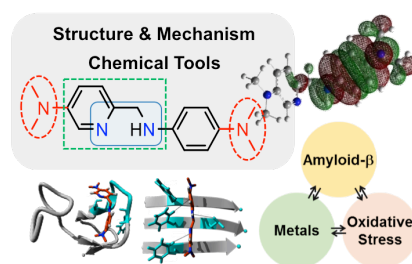
- [1] a) R. Jakob-Roetne, H. Jacobsen, *Angew. Chem. Int. Ed.* **2009**, *48*, 3030-3059; b) K. P. Kepp, *Chem. Rev.* **2012**, *112*, 5193-5239; c) C. Rodriguez-Rodriguez, M. Telpoukhovskaia, C. Orvig, *Coord. Chem. Rev.* **2012**, *256*, 2308-2332; d) M. W. Beck, A. S. Pithadia, A. S. DeToma, K. J. Korshavn, M. H. Lim in *Ligand Design in Medicinal Inorganic Chemistry* (Ed.: T. Storr), Wiley, Chichester, **2014**, Chapter 10, pp. 256-286.
- [2] a) K. Ono, M. M. Cordron, D. B. Teplow, *Proc. Natl. Acad. Sci. USA* **2009**, *106*, 14745-14750; b) C. Haass, D. J. Selkoe, *Nat. Rev. Mol. Cell Biol.* **2007**, *8*, 101-112; c) K. P. Kepp, *J. Alzheimers Dis.* **2016**, *56*, 1-11.
- [3] a) J. A. Duce, A. I. Bush, *Prog. Neurobiol.* **2010**, *92*, 1-18; b) E. L. Que, D. W. Domaille, C. J. Chang, *Chem. Rev.* **2008**, *108*, 1517-1549; c) P. Zatta, D. Drago, S. Bolognin, S. L. Sensi, *Trends Pharmacol. Sci.* **2009**, *30*, 346-355; d) P. Faller, *ChemBioChem* **2009**, *10*, 2837-2845; e) S. Chassaing, F. Collin, P. Dorlet, J. Gout, C. Hureau, P. Faller, *Curr. Top. Med. Chem.* **2012**, *12*, 2573-2595; f) A. A. Belaidi, A. I. Bush, *J. Neurochem.* **2016**, *139*, 179-197.
- [4] a) S. S. Hindo, A. M. Mancino, J. J. Braymer, Y. Liu, S. Vivekanandan, A. Ramamoorthy, M. H. Lim, *J. Am. Chem. Soc.* **2009**, *131*, 16663-16665; b) J.-S. Choi, J. J. Braymer, R. P. Nanga, A. Ramamoorthy, M. H. Lim, *Proc. Natl. Acad. Sci. USA* **2010**, *107*, 21990-21995; c) J. S. Derrick, R. A. Kerr, K. J. Korshavn, M. J. McLane, J. Kang, E. Nam, A. Ramamoorthy, B. T. Ruotolo, M. H. Lim, *Inorg. Chem.* **2016**, *55*, 5000-5013; d) S. Lee, X. Zheng, J. Krishnamoorthy, M. G. Savelieff, H. M. Park, J. R. Brender, J. H. Kim, J. S. Derrick, A. Kochi, H. J. Lee, C. Kim, A. Ramamoorthy, M. T. Bowers, M. H. Lim, *J. Am. Chem. Soc.* **2014**, *136*, 299-310; e) M. G. Savelieff, Y. Liu, R. R. Senthamarai, K. J. Korshavn, H. J. Lee, A. Ramamoorthy, M. H. Lim, *Chem. Commun.* **2014**, *50*, 5301-5303; f) M. W. Beck, S. B. Oh, R. A. Kerr, H. J. Lee, S. H. Kim, S. Kim, M. Jang, B. T. Ruotolo, J.-Y. Lee, M. H. Lim, *Chem. Sci.* **2015**, *6*, 1879-1886; g) J. S. Derrick, R. A. Kerr, Y. Nam, S. B. Oh, H. J. Lee, K. G. Earnest, N. Suh, K. L. Peck, M. Ozbil, K. J. Korshavn, A. Ramamoorthy, R. Prabhakar, E. J. Merino, J. Shearer, J.-Y. Lee, B. T. Ruotolo, M. H. Lim, *J. Am. Chem. Soc.* **2015**, *137*, 14785-14797; h) A. K. Sharma, S. T. Pavlova, J. Kim, D. Finkelstein, N. J. Hawco, N. P. Rath, J. Kim, L. M. Mirica, *J. Am. Chem. Soc.* **2012**, *134*, 6625-6636; i) C. Rodriguez-Rodriguez, N. Sanchez de Groot, A. Rimola, A. Alvarez-Larena, V. Lloveras, J. Vidal-Gancedo, S. Ventura, J. Vendrell, M. Sodupe, P. Gonzalez-Duarte, *J. Am. Chem. Soc.* **2009**, *131*, 1436-1451.
- [5] H. F. Kung, C. W. Lee, Z. P. Zhuang, M. P. Kung, C. Hou, K. Plossl, *J. Am. Chem. Soc.* **2001**, *123*, 12740-12741.
- [6] a) A. Avdeef, S. Bendels, L. Di, B. Faller, M. Kansy, K. Sugano, Y. Yamauchi, *J. Pharm. Sci.* **2007**, *96*, 2893-2909; b) *BBB Protocol and Test Compounds*, pION Inc., **2009**.
- [7] a) R. Re, N. Pellegrini, A. Proteggente, A. Pannala, M. Yang, C. Rice-Evans, *Free Radic. Biol. Med.* **1999**, *26*, 1231-1237; b) H. Schugar, D. E. Green, M. L. Bowen, L. E. Scott, T. Storr, K. Bohmerle, F. Thomas, D. D. Allen, P. R. Lockman, M. Merkel, K. H. Thompson, C. Orvig, *Angew. Chem. Int. Ed.* **2007**, *46*, 1716-1718.
- [8] M. Coles, W. Bicknell, A. A. Watson, D. P. Fairlie, D. J. Craik, *Biochemistry* **1998**, *37*, 11064-11077.
- [9] O. Trott, A. J. Olson, *J. Comput. Chem.* **2010**, *31*, 455-461.
- [10] a) C. Oostenbrink, A. Villa, A. E. Mark, W. F. Van Gunsteren, *J. Comput. Chem.* **2004**, *25*, 1656-1676; b) D. A. Case, T. E. Cheatham III, T. Darden, H. Gohlke, R. Luo, K. M. Merz Jr., A. Onufriev, C. Simmerling, B. Wang, R. J. Woods, *J. Comput. Chem.* **2005**, *26*, 1668-1688; c) E. Lindahl, B. Hess, *J. Mol. Model* **2001**, *7*, 306-317.
- [11] M. Mayer, B. Meyer, *J. Am. Chem. Soc.* **2001**, *123*, 6108-6117.
- [12] A. T. Petkova, W. M. Yau, R. Tycko, *Biochemistry* **2006**, *45*, 498-512.
- [13] a) H. Hernandez, C. V. Robinson, *Nat. Protoc.* **2007**, *2*, 715-726; b) G. R. Hilton, J. L. Benesch, *J. R. Soc. Interface* **2012**, *9*, 801-816.
- [14] a) C. L. Hawkins, M. J. Davies, *Biochim. Biophys. Acta* **2001**, *1504*, 196-219; b) W. M. Garrison, *Chem. Rev.* **1987**, *87*, 381-398; c) M. R. Porter, A. Kochi, J. A. Karty, M. H. Lim, J. M. Zaleski, *Chem. Sci.* **2015**, *6*, 1018-1026; d) M. W. Beck, J. S. Derrick, R. A. Kerr, S. B. Oh, W. J. Cho, S. J. C. Lee, Y. Ji, J. Han, Z. S. Tehrani, N. Suh, S. Kim, S. D. Larsen, K. S. Kim, J.-Y. Lee, B. T. Ruotolo M. H. Lim, *Nat. Commun.* **2016**, *7*, 13115.

FULL PAPER
FULL PAPER

WILEY-VCH

Inventing smart chemical tools:

A structure-mechanism-based design strategy is demonstrated to be useful for inventing chemical tools able to constructing the actions of diverse pathological factors in Alzheimer's disease.



Dr. Hyuck Jin Lee, Dr. Kyle J. Korshavn, Younwoo Nam, Juhye Kang, Thomas J. Paul, Dr. Richard A. Kerr, Dr. Il Seung Youn, Dr. Mehmet Ozbil, Prof. Dr. Kwang S. Kim, Prof. Dr. Brandon T. Ruotolo, Prof. Dr. Rajeev Prabhakar,* Prof. Dr. Ayyalusamy Ramamoorthy* and Prof. Dr. Mi Hee Lim*

Page No. – Page No.

Structural and Mechanistic Insights into Development of Chemical Tools to Control Individual and Inter-related Pathological Features in